

Challenges in the first-principles description of reactions in electrocatalysis

Sebastian Schnur and Axel Groß

Institut für Theoretische Chemie, Universität Ulm, D-89069 Ulm, Germany

In spite of the strong relevance of reactions in electrocatalysis, in particular for the electrochemical energy conversion and storage, the number of theoretical studies addressing electrocatalytic reaction from first principles is still limited. This is due to the fact that there are two factors adding considerable complexity to the theoretical treatment: the presence of the electrolyte at the electrode surface and varying electrode potentials. Still, there are promising approaches to cope with these problems allowing a realistic theoretical description of reactions in electrocatalysis. It will be demonstrated that *ab initio* molecular dynamics simulations based on periodic density functional theory calculations can contribute to an understanding of the structures and reactions at water/metal interfaces. In order to model varying electrode potentials, an explicit counter electrode has been implemented in a periodic density functional theory code, and first preliminary results using this implementation will be presented.

I. INTRODUCTION

There is currently a strong interest in reactions in electrocatalysis due to the fact that they play a very important role in the electrochemical energy conversion or storage. However, in spite of considerable research efforts it is fair to say that still the details of important, but seemingly simple reactions in electrocatalysis such as the oxygen reduction reaction (ORR) or the hydrogen evolution reaction (HER) are debated [1–3].

In the field of surface science, on the other hand, recent years have witnessed a close collaboration between theory and experiment resulting in detailed insights into structures and reactions at the solid/vacuum interface [4–8]. The theoretical description of electrochemical interfaces, however, is hampered by two factors: the presence of the electrolyte at the electrode surface and varying electrode potentials. Both factors add considerable complexity to the theoretical and numerical treatment of these interfaces. Yet, there is certainly a strong need for reliable first-principles studies of structures and processes at electrochemical interfaces in order to understand the principles underlying these structures and processes.

In fact, there have already been several attempts to realistically model the electrochemical solid-liquid interface within periodic DFT calculations [9–18] providing valuable insights into fundamental electrochemical processes at the atomistic level. Interestingly enough, there is yet no commonly used method to describe varying electrode potentials in periodic DFT calculations. This is an indication that the first-principles description of electrochemical processes has not matured yet.

One particularly important reaction in electrocatalysis is the hydrogen evolution/oxidation [1]. Recently, we mapped out a two-dimensional cut through the potential energy surface of H_2 interacting with clean and ice-covered Pt(111) [19]. Because of the weak water-metal interaction, the dissociation barrier in the presence of water can be regarded as a superposition of the dissociation barrier on the clean Pt(111) surface and the barrier for the propagation of H_2 through the ice-like layer. Fur-

thermore, we studied the structure of water layers at the (111) surfaces of various metal substrate at room temperature using *ab initio* molecular dynamics simulations [20]. According to the simulations, water does not remain ice-like in so-called H-up or H-down structures, as was commonly assumed [21], but becomes disordered. On more strongly interacting electrodes such as Pt(111), Ru(111) and Pd/Au(111), a hexagonal ordering might persist, but the orientation of the water molecules becomes random, whereas on more weakly interacting substrates such as Ag or Au, even no periodic ordering remains.

We have now extended this work by studying the H_2 dissociation on ice-covered Ru(0001) and Pd/Au(111) in order to determine the influence of the lattice spacing on the H_2 dissociation barrier in the presence of water. Considering that at room temperature the water structure at these electrodes is not ice-like, we have also calculated free energy barriers by performing a statistical sampling at room temperature.

In these studies, there is no external electric field considered. To take into account the influence of varying electrode potentials, we have performed an analysis of the Heyrovsky reaction in the spirit of the approach by Nørskov and coworkers [14, 22]. Finally, the implementation of an explicit counter electrode in a periodic DFT code is described and first results using this implementation are presented.

II. COMPUTATIONAL METHODS

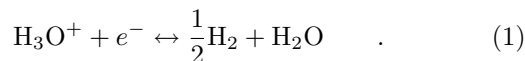
All total-energy calculations were carried out using the periodic DFT package VASP [23], employing the generalized gradient approximation (GGA) to describe the exchange-correlation effects by employing the exchange-correlation functional by Perdew, Burke and Ernzerhof (PBE) [24]. It has been shown that this functional gives a reasonable description of the properties of water [25–27]. The ionic cores were represented by projector augmented wave (PAW) potentials [28] as constructed by Kresse and Joubert [29]. The electronic one-particle wave function were expanded in a plane-wave basis set up to an energy

cutoff of 400 eV. The metal substrates were represented by four- and five-layer slabs.

Ab initio molecular dynamics (AIMD) simulations were performed using the Verlet algorithm with a time step of 1 fs at a temperature of 300 K within the micro-canonical ensemble.

III. HYDROGEN DISSOCIATION AT WATER-COVERED METAL SURFACES

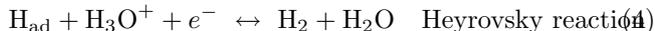
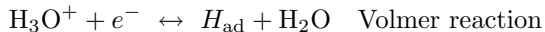
The hydrogen evolution and oxidation reactions, HER and HOR, respectively, play a central role in many important electrocatalytic processes as they occur, e.g., in fuel cells. Under acidic conditions, the overall reaction can be written as



There are two basic reaction schemes depending on the nature of the electrodes. In the Volmer-Tafel-mechanism,



first a proton adsorbs taking up an electron from the electrode (Volmer step). In a second step, two hydrogen atoms desorb recombinatively (Tafel step). In the Volmer-Heyrovsky-mechanism



again first a Volmer step occurs, but then an adsorbed hydrogen atom reacts with a solvated proton forming H_2 gas and water (Heyrovsky step).

We will first focus on the Tafel mechanism which has a close correspondence to the dissociative adsorption and recombinative desorption of hydrogen at the metal-vacuum interface. There, hydrogen typically adsorbs dissociatively [30], only at stepped metal surfaces, nondissociative molecular adsorption might occur [31]. Recently, we showed that the barrier for the dissociative adsorption of hydrogen at an ice-covered surface can be regarded as being a superposition of the dissociation barrier on the clean Pt(111) surface and the barrier for the propagation of H_2 through the ice-like layer [19]. The propagation of H_2 through a hexagonal ice layer is hindered due to the Pauli repulsion between H_2 and water. Consequently, this barrier should depend on the diameter of the hexagonal ice ring.

In order to test this hypothesis, we calculated two-dimensional cuts through the potential energy surfaces of H_2 interacting with clean and ice-covered Ru(0001) and Pd/Au(111) as a function of the H-H separation and the H_2 distance from the surface, so-called elbow plots [32]. Ru has a nearest-neighbor distance which is about 0.1 Å smaller than the one of Pt. The Pd/Au(111) electrode

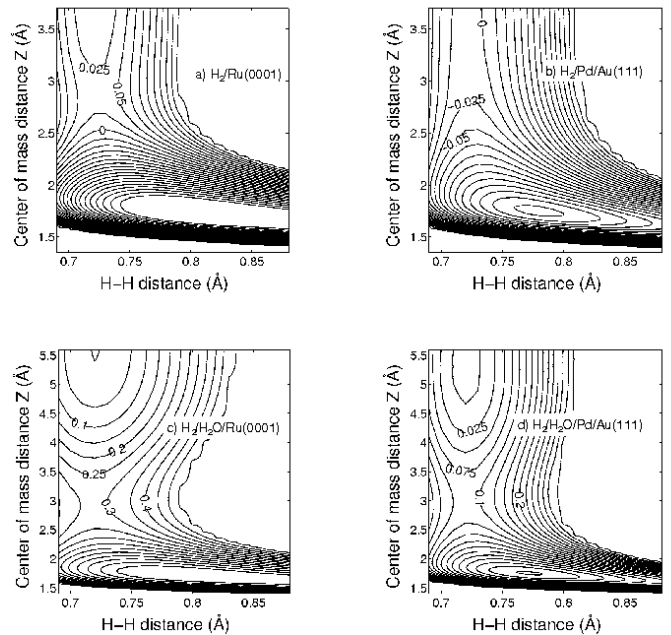


FIG. 1: Two-dimensional cuts through the potential energy surface of the interaction of H_2 with clean Ru(0001) (a), clean Pd/Au(111) (b), ice-covered Ru(0001) (c), and ice-covered Pd/Au(111). The ice-like water bilayer is in the H-down configuration. The potential energy is plotted as a function of the H-H distance d and the H_2 center of mass distance Z from the surface. The lateral position and orientation of the H_2 molecule correspond to a fcc hollow-top-hcp hollow configuration. The contour spacing in (a), (b) and (d) is 25 meV, while it is 50 meV in (c).

consisting of a pseudomorphic Pd layer on Au(111) was chosen because it has the nearest-neighbor distance of Au (about 0.1 Å larger than the one of Pt), but a local reactivity that is even larger than the one of Pd(111) [33–36]. Here we assume that the ice layer adsorbs pseudomorphically on the electrodes within a $\sqrt{3} \times \sqrt{3}R30^\circ$ geometry.

In Fig. 1, we have plotted the elbow plots of H_2 interacting with clean and water-covered Ru(0001) and Pd/Au(111). The lateral position and orientation of the H_2 molecule correspond to a fcc hollow-top-hcp hollow configuration, i.e., the center of mass of the H_2 molecule is located above a top position, and the H atoms are oriented towards the nearest three-fold hollow sites.

The corresponding barrier heights together with the values for Pt(111) [19] are collected in Tab. I. Hydrogen dissociation on clean Pt(111) and Ru(0001) is hindered by a small barrier, whereas on Pd/Au(111), H_2 can dissociate spontaneously. On Pt(111), the presence of the water bilayer leads to an increase of the dissociation barrier by about 170 meV. Indeed, on Ru(0001) the smaller nearest neighbor distance compared to Pt causes an even larger increase of the H_2 dissociation barrier by 260 meV due to the presence of the ordered water bilayer.

For clean Pd/Au(111), there is no minimum H_2 dissociation barrier while in the presence of water a barrier of

TABLE I: H₂ dissociation barriers on clean and ice-covered metal surfaces

Substrate	Water structure	ΔE (meV)	z (Å)	Metal NN distance (Å)
Pt(111)	clean	54	2.4	2.77
Pt(111)	H-down	221	2.5	
Ru(0001)	clean	30	2.8	
Ru(0001)	H-down	290	3.0	2.68
Ru(0001)	H-up	369	2.8	
Pd/Au(111)	clean	0	-	2.86
Pd/Au(111)	H-down	91	3.0	

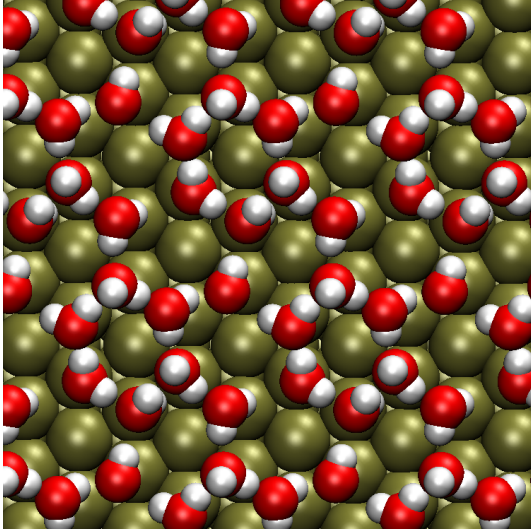


FIG. 2: Snapshot of an ab initio molecular dynamics run at 7.5 ps of a water bilayer on a Pt(111) electrode at a temperature of 300 K. The simulations were initiated with a H-down configuration within a $2\sqrt{3} \times 2\sqrt{3}R30^\circ$ geometry [20].

91 meV appears. At the location of this barrier, this corresponds to an increase of the potential energy of about 100 meV. Hence, we find a strong correlation between the increase in the H₂ dissociation barrier due to the presence of an ordered water bilayer and the diameter of the hexagonal rings of the bilayer. Note that the electronic structure of metal substrates is only weakly perturbed by an adsorbed water layer [19]. This supports our findings that the increase of the H₂ dissociation barrier in the presence of water is not caused by a water-induced modification of the electronic structure of the electrode, but rather by an additional effect caused by the Pauli repulsion between H₂ and the water layer.

All the calculations presented so far have been done for ice-like water layers on close-packed electrode surfaces. However, ab initio molecular dynamics simulations indicate that at room temperature water layers at metal surfaces are not crystalline but disordered [20]. This is illustrated in Fig. 2 where a snapshot of an ab initio molecular dynamics run of a water layer on Pt(111) within a $2\sqrt{3} \times 2\sqrt{3}R30^\circ$ geometry is shown. Still a hexagonal structure of the water molecules is visible but there is no

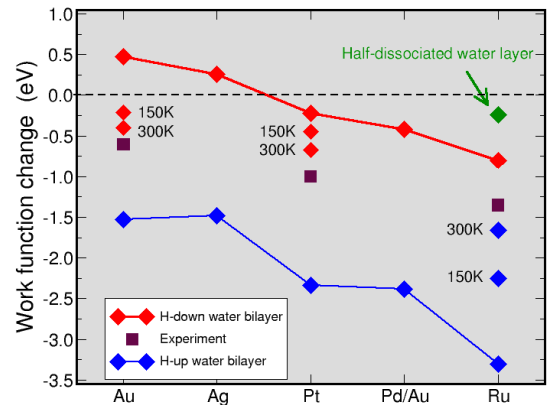


FIG. 3: Calculated work function change induced by the presence of H-up and H-down water bilayers on Au(111), Ag(111), Pt(111), Pd/Au(111) and Ru(0001). For Ru, also the work function change induced by the half-dissociated water layer is included. In addition, the time average of the work function change determined in AIMD runs with a run time of 2 ps at 150 K and 300 K is plotted and compared to experimental results for Au(111) [37], Pt(111) [38, 39] and Ru(0001) [40, 41].

orientational order of the water molecules.

This orientational disorder has a considerable influence on the work function change upon the adsorption of a water layer on metal substrates. For ice-like water layers, there is a significant difference in the work function change upon the adsorption of H-up and H-down layers which is due to the opposite dipole moment of these structures [20]. This is illustrated in Fig. 3. Note that there is also a strong polarization of the ice-like layers upon adsorption which leads to a charge transfer from the ice layer to the region between the metal and the ice layer and consequently to an additional downshift of the work function which is related to the strength of the water-metal interaction [20]. However, there is a rather large discrepancy between the calculated work function change for the ice-like layers and the experimental results for Au(111) [37], Pt(111) [38, 39] and Ru(0001) [40, 41]. However, this discrepancy is strongly reduced if then thermal motion of the water molecules is taken into account. This has been done by running AIMD simulations

for 2 ps at 150 K and 300 K and evaluating the average work function change. Although the run time is not sufficient to obtain fully converged results, it is obvious that the thermal motion of the water molecules and the accompanying reorientation leads to work function changes that are intermediate between the corresponding values for the H-down and H-up layer. In fact, longer runs have shown that the resulting work function changes are independent of the initial conditions, i.e., there is no memory effect as far as the structure is concerned.

In passing we note that for Ru(0001) there is a good agreement between the experiment and the theoretical results for finite temperatures for the intact water layer. In contrast, the half-dissociated water layer exhibits a much smaller work function change in the calculations which remains basically unchanged at finite temperature due to much larger binding of the OH groups which pins the water structures. Thus, although the half-dissociated water layer on Ru is energetically much more favorable [21, 42, 43], it does not seem to be realized in surface science experiments, probably due to kinetic hindering [43–45].

The bad news for the modeling of structures and processes at the solid-liquid interface is that these findings with respect to the water structures at room temperature mean that it is not sufficient to determine energy minimum structures and transition states. Instead of total energies, free energies have to be evaluated which involves the consideration of statistical averages. To do this from first principles is typically numerically rather time consuming. Still, due to the increase in the computer power and the development of efficient algorithms, ab initio molecular dynamics runs nowadays allow the determination of statistically meaningful results [46].

In order to estimate the free energies along the dissociation path of H_2 in the presence of water, we performed constraint ab initio molecular dynamics simulations in the spirit of umbrella sampling [47, 48]. The initial conditions were chosen along the minimum energy path derived from the elbow plots shown in Fig. 1. In the constraint AIMD simulations, the height of the two hydrogen atoms above the surface was fixed, and simulations were performed within the microcanonical ensemble corresponding to a temperature of 300 K. The AIMD runs were carried out for 2 ps and the average energies were determined.

These energies as a function of the H_2 distance from the Pt(111), Ru(0001) and Pd/Au(111) are plotted in Fig. 4. It is apparent that the resulting free energy curves are not smooth indicating that the free energy sampling might not be converged yet. Still the qualitative trends due to the thermal averaging can be deduced from the curves. The energy zero corresponds to the free energy of the H_2 molecule at 6.5 Å away from the surface above the water layer. Note that there is a very small interaction between the H_2 molecule and the water molecules at a position between two ice-like layers [19] which is reflected by the small solvation energy of H_2 in water. Hence this

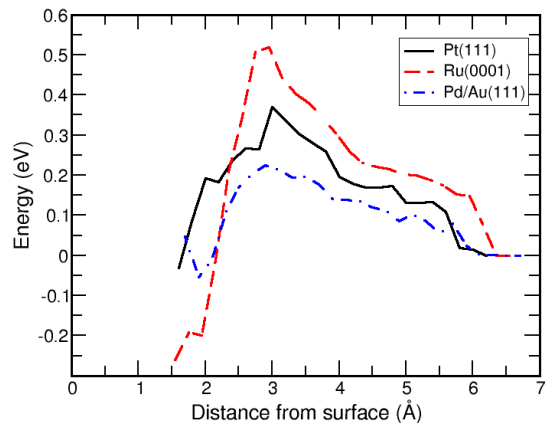


FIG. 4: Free energies along the H_2 dissociation path on water-covered Pt(111), Ru(0001) and Pd/Au(111) at 300 K obtained by constraint AIMD runs with a run time of 2 ps.

choice of the energy zero should be adequate.

At all three surfaces, the free energy barriers in the presence of water are about 150 meV higher at room temperature than for the ice-like hexagonal structure. This is due to the irregular shape of the hexagonal water rings under thermal conditions which makes the propagation of the H_2 molecule through the water layer even harder.

IV. MODELLING OF VARYING ELECTRODE POTENTIALS

So far, all the presented calculations have been carried out for neutral systems which means that no excess charges were considered. However, any realistic theoretical description of electrochemical systems requires the consideration of varying electrode potentials and the accompanying excess charges. Still, important trends for electrochemical systems can already be derived without an explicit consideration of external electric fields or any excess charges employing thermodynamical equilibrium concepts [22].

We will illustrate this approach using the adsorption of hydrogen atoms as part of the Volmer reaction 2. Here we follow the approach by Skulason *et al.* [14]. The hydrogen coverage on a platinum electrode is a function of the electrode potential and the hydrogen adsorption energies. In Tab. II, the hydrogen adsorption energies with respect to the free H_2 molecule,

$$E_{H_{ad}} = E_{H/electrode} - \left(E_{electrode} + \frac{1}{2} E_{H_2} \right), \quad (5)$$

on different metal electrodes in the presence and absence of ice-like water bilayers are listed. First of all it is evident that the presence of water has a relatively small effect on the hydrogen adsorption energies, as already

observed before [10, 49]. This is a consequence of the weak interaction of water with metal surfaces [19].

Among the considered metal substrates, Pt(111) plays a special role. First of all, the hydrogen adsorption energies exhibit a surprisingly small corrugation with the adsorption at the top sites as strong as on the three-fold hollow sites. Second, at the ice-covered Pt(111) the hydrogen atoms at the top site directly beneath the oxygen atom of the flat lying water molecule (denoted by site top(b) in Tab. II) are more stable than those at the top site not covered by water (top(a)). On all other considered metal substrates, it is the other way around (not listed in Tab. II)).

At equilibrium, the resulting hydrogen coverage of hydrogen on the electrode is a function of the electrode potential related to the hydrogen adsorption energies. At the equilibrium potential under standard conditions, the chemical potential of the hydrogen atoms is related to the electrode potential with respect to the normal water electrode by

$$\mu_{\text{H}} = -eU . \quad (6)$$

All processes with a change of the free energy $\Delta G_{\text{H}} < \mu_{\text{H}} = -eU$ occur under equilibrium conditions. This means, that the differential free energy of adsorption is directly related to the hydrogen coverage of the electrode [14]. Assuming that the adsorption energy is not dependent on the applied electrode potential, this differ-

TABLE II: Adsorption energies of hydrogen according to Eq. (5) on different adsorption sites on Au(111), Ag(111), Pt(111), Pd/Au(111) and Ru(0001) in a $\sqrt{3} \times \sqrt{3}R30^\circ$ geometry with respect to the free H_2 molecule in eV per atom in the presence and absence of ice-like water bilayers. The top site for the H atom in the presence of water corresponds to the site uncovered by water. In the case of Pt(111), in addition the site directly beneath the oxygen atom of the flat lying water molecule is considered (top(b)).

Surface	adsorption site	H-down	H-up	clean
Ru(0001)	fcc	-0.489	-0.483	-0.614
Ru(0001)	hcp	-0.461	-0.421	-0.561
Ru(0001)	top	-0.153	-0.247	-0.148
Ag(111)	fcc	0.235	0.195	0.180
Ag(111)	hcp	0.223	0.207	0.174
Ag(111)	top	0.729	0.669	0.691
Au(111)	fcc	0.265	0.167	0.203
Au(111)	hcp	0.238	0.138	0.222
Au(111)	top	0.367	0.310	0.399
Pd/Au(111)	fcc	-0.623	-0.724	-0.696
Pd/Au(111)	hcp	-0.566	-0.669	-0.650
Pd/Au(111)	top	0.112	0.070	0.040
Pt(111)	fcc	-0.412	-0.427	-0.477
Pt(111)	hcp	-0.336	-0.370	-0.438
Pt(111)	top(a)	-0.375	-0.382	-0.480
Pt(111)	top(b)	-0.463	-0.405	-0.480

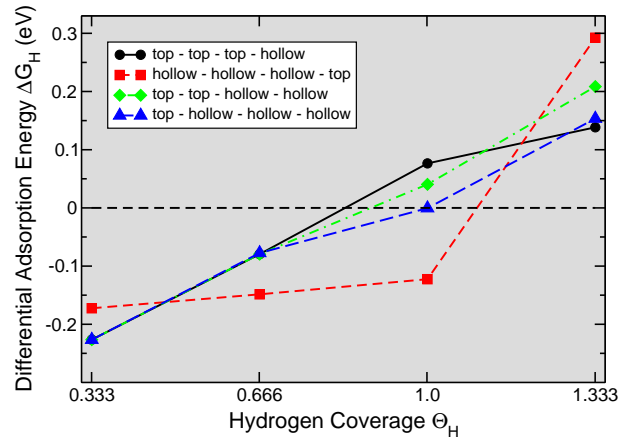


FIG. 5: Differential free energy of adsorption of hydrogen as a function of the hydrogen coverage on ice-covered Pt(111) in a $\sqrt{3} \times \sqrt{3}R30^\circ$ geometry. The adsorption site sequence is indicated in the legends.

ential free energy of adsorption can be expressed as [22]

$$\Delta G_{\text{H}} = \Delta E_{\text{H}} + \Delta ZPE - T\Delta S . \quad (7)$$

Here, ΔE_{H} is the differential energy of adsorption in the absence of any external electric fields, i.e., the energy gain upon the adsorption of an additional hydrogen atom. ΔZPE is the change of the zero-point energy upon adsorption, T the temperature and ΔS the change of the entropy upon adsorption. For hydrogen on Cu(111), a value of $\Delta ZPE - T\Delta S = -0.24 \text{ eV}$ has been determined [50]. As previously done, we will also use this value for other substrates based on the observation that the change of vibrational frequencies upon adsorption depends rather weakly on the metal substrate [51].

The differential adsorption energies of hydrogen atoms on Pt(111) in the presence of a water layer are plotted in Fig. 5 for different adsorption site sequences. These results are in good agreement with previously calculated differential adsorption energies which were, however, determined for different coverages [14]. The minimum value $\Delta G_{\text{H}}(\Theta_{\text{H}} = 1/3) = -0.225 \text{ eV}$ means that at $U = 0.225 \text{ V}$ a hydrogen coverage of $\Theta_{\text{H}} = 1/3$ is stable. This compares quite favorably with the value of $U = 0.15 - 0.2 \text{ V}$ for this coverage which can be deduced from experimentally derived adsorption isotherms [52].

Interestingly enough, at this coverage the most favorable adsorption site is the top site. For higher coverages, the adsorption in the three-fold hollow positions becomes more favorable. Because of the small hydrogen diffusion barriers, the rearrangement of the hydrogen atoms should not be kinetically hindered. According to Fig. 5, at $U = 0.0 \text{ V}$ a coverage of $\Theta_{\text{H}} = 1$ is expected. This seems to be at variance with the experimentally observed hydrogen saturation coverage of $\Theta_{\text{H}} = 2/3$ at $U = 0.0 \text{ V}$ [1]. However, this discrepancy is reduced if the configurational entropy is also taken into account in the calculated free energies [14].

For $\Theta_{\text{H}} \leq 1$, the change in the differential adsorption energies at the hollow sites is of the order of 0.04 eV indicating a relatively small mutual repulsion between the hydrogen atoms at the hollow sites. For hydrogen coverages larger than one monolayer, the repulsion increases significantly leading to differential adsorption energies larger than 0 eV. Thus additional hydrogen at coverages larger than one can only be adsorbed below the equilibrium potential. This hydrogen species is called overpotential deposited hydrogen H_{opd} , in contrast to underpotential deposited hydrogen H_{upd} which adsorbs at potentials above the equilibrium potential.

Experimentally, in the H_{upd} regime a broad vibrational band around 1000-1300 cm^{-1} has been found by infrared reflection-absorption spectroscopy (IRAS) [53] whereas at the equilibrium potential a new peak at 2100 cm^{-1} appears whose intensity increases linearly with decreasing potential [54]; therefore it has been associated with H_{opd} . Like others before [14], we have derived the vibrational frequencies of hydrogen at the different adsorption sites from the dynamical matrix. For three-fold coordinated hydrogen, we find a frequency of 1062 cm^{-1} confirming the site assignment of the upd hydrogen.

At the top site, we obtain vibrational frequencies of 2029 cm^{-1} and 2267 cm^{-1} at water-covered and uncovered Pt atoms, respectively. However, according to the calculations, at $\Theta_{\text{H}} = 1$ the top sites should not be populated so that no signal at these high frequencies should be detectable. It has been speculated, that the top site corresponds to a thermally populated minority species that has a much larger dynamical dipole matrix elements and therefore becomes detectable [14]. In order to check whether the top site population of hydrogen occurs under thermal conditions, we performed ab initio molecular dynamics simulations at a temperature of 300 K in a setup as used previously [20]: two water layers were considered in a $2\sqrt{3} \times 2\sqrt{3}R30^\circ$ geometry with hydrogen atoms initially at the energetically more favorable hollow positions. An additional hydrogen atom was incorporated in the water layer becoming a solvated proton because otherwise the adsorbed hydrogen atoms tend to desorb. The vibrational spectrum was derived by evaluating the Fourier transform of the velocity autocorrelation function.

Two different hydrogen coverages were considered, $\Theta_{\text{H}} = 2/3$ and $\Theta_{\text{H}} = 1$. A peak at about 2100 cm^{-1} was only detectable at the lower coverage, not at the higher coverage. This can be understood considering the strong repulsion between hydrogen at hollow sites and at adjacent top sites which is operative at a monolayer coverage of hydrogen. At a smaller coverage, there are regions of low local hydrogen coverage allowing hydrogen top site adsorption. Hence, at coverages around $\Theta_{\text{H}} = 1$, inhomogeneities in the hydrogen distribution are required so that the top sites can be populated by hydrogen atoms.

In all the considerations presented in this section so far it was assumed that any electric field caused by the applied electrode potential and any excess charges on the

electrodes do not have any influence on the adsorption energies and adsorption site preferences. There are indications that at least qualitatively the effect of this additional factors might be small [22]. Still, it is desirable to achieve a realistic modelling of the electrochemical electrode/electrolyte interface in order to be able to assess the magnitude of these effects. In fact, there have been several attempts to include the effects of external electric fields or excess charges in periodic DFT calculations.

In standard DFT calculations, a dipole layer is introduced in the vacuum region between two slabs in order to avoid electric field effects due to non-symmetric slabs in periodic DFT slab calculations, [55]. This dipole layer can also be used to create a specified electric field as done in order to study the field-induced flip of water molecules from the H-down configuration to the H-up geometry [10]. This approach does not introduce any excess charges so that charge neutrality is maintained, but it is not straightforward to relate the applied dipole field to the corresponding electrode potential. Furthermore, it is not easy to specify the excess charge at the electrode surface induced by the electric field.

In principle, it is no problem to consider charged systems in periodic DFT calculations. However, due to the fact that the energy of a charged infinite periodic system diverges, any excess charge has to be counterbalanced. Typically, a neutralizing charge background is automatically assumed in periodic DFT calculations by omitting the $\mathbf{G} = 0$ term in the Fourier expansion of the electrostatic energy. However, an uniform charge background can lead to artefacts in the one-electron potential, namely a quadratically varying potential [12]. On the other hand, the influence of this artefact is strongly reduced due to screening effects in regions such as at the metal-water interface where polarizable atoms and molecules are present [12]. This makes this approach applicable for the description of processes at electrochemical interfaces [11, 12, 56, 57]. Still, another problem is present. Because of the absence of any charge-free vacuum region, there is no direct way to specify the work function and thus the electrode potential. Still it is possible to derive the corresponding electrode potentials invoking a so-called double reference method [12]. Furthermore, the total energy has to be corrected with respect to the electrostatic interaction of the ions and electrons with the uniform charge background.

An elegant method that avoids the introduction of additional charges has been proposed by Rossmeisl, Nørskov and coworkers [14, 18]. In this approach, neutral atoms or molecules that act as electron donors or acceptors are explicitly added to the electrolyte. So far, this has been done by introducing additional hydrogen atoms to the water-metal interface [14, 18] leading to solvated protons whereas the electrons move to the metal electrode since there are empty states at the Fermi energy. By changing the hydrogen concentration, the surface charge and hence the electrode potential can be varied. This leads to a realistic description of the electrochemical in-

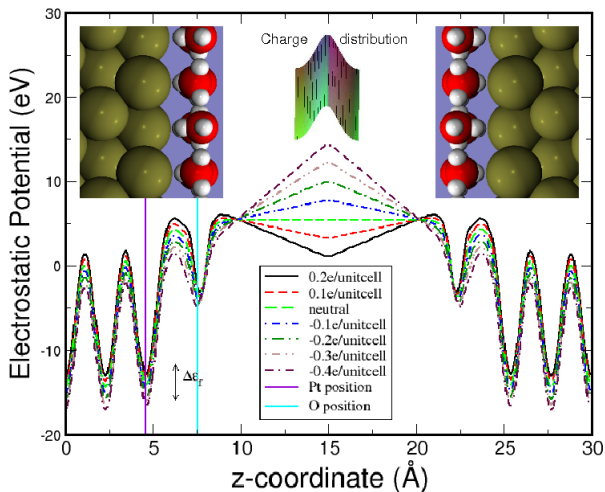


FIG. 6: Laterally averaged one-electron potential of a symmetrically constructed metal-water slab for varying electron numbers and explicit Gaussian-shaped counter electrode in the middle of the supercell.

interface since the excess charge at the electrode is balanced by counter ions in the Helmholtz layer. Still, these counter ions might directly interact with any reacting species so that it is hard to disentangle electric field effects from interaction effects which is a prerequisite for an understanding of the fundamental factors underlying electrocatalysis.

As an alternative approach, a counter electrode may be explicitly considered, for example as a localized planar charge distribution with a Gaussian profile perpendicular to the surface [15, 58–61] or by putting a perfect conducting continuum with a non-vanishing surface charge above the slab in a two-dimensional periodic approach [13, 16, 17]. Thus the reconstruction of charged surfaces [58, 59, 61] or the structure of water under acidic conditions [16, 17] was addressed. This approach allows to disentangle field-induced effects from coverage effects. Furthermore, it avoids any artefacts in the one-electron potential due to the presence of the uniform charge background anywhere in space. In order to determine the electrode potential in this method, the charge can be related to the potential via experimentally derived capacities [59] or in the presence of several water layers from the potential profile inside of the water bulk region [17].

We have implemented such a Gaussian-shaped counter electrode

$$\rho_{ce}(\mathbf{r}) = \frac{q}{\sqrt{2\pi}\sigma} \exp\left(-\frac{z-z_0}{2\sigma}\right)^2, \quad (8)$$

in the VASP code [23]. Here q is the total charge of the counter electrode and z_0 corresponds to the position of the counter electrode. The width of the Gaussian charge distribution is given by σ which has been chosen to be numerically convenient. In practice, $\sigma = 0.1 \text{ \AA}$ is sufficient to avoid any error due to the discretization of the

charge in reciprocal space. The resulting laterally averaged one-electron potentials for different excess electron numbers for a symmetric slab covered by one water-layer are illustrated in Fig. 6. Note that the excess charge due to the additional electrons is exactly compensated by the counter electrode.

Inside the metal slab, the potential is just shifted due to the screening of the electric field at the metal surface. The electric field strength in the vacuum region can be deduced from the slope of the linear regions. It is obvious that there is an upper limit of the charge of the counter electrode for positive charge. If this charge becomes large enough that the potential in the regions between the slabs drops below the Fermi energy, there would be an artificial electron transfer from the metal slabs to the counter electrode. Note that although the counter electrode and the considered atoms are separated in space, there is still a direct electrostatic interaction between the electrons and the ion core with the counter electrode. The resulting total energy has to be corrected for this interaction. This is done in an analogous way as described by Taylor *et al.* [12]. Furthermore, the energy has also to be corrected to account for the different number of electrons in each system. The electrons are assumed to be in equilibrium with a reservoir given by the electrochemical potential μ . Thus the total grand canonical free energy, except for entropic effects is given by

$$E_{\text{free}} = E + \mu q, \quad (9)$$

where E is the total energy from the DFT calculations corrected for the electrostatic interaction with the counter electrode, and q is the total charge of the electron-ion system. The electrochemical potential μ has been taken with respect to the reference system with $q = 0$.

It is obvious from Fig. 6 that there is no extended field-free region in this implementation so that no vacuum level can be defined. This also means that no work function and hence no electrode potential [62] can be directly deduced. Our implementation shares this problem with the approach in which the counter electrode is represented by a uniform compensating charge background. For this latter approach, a double-reference method to specify the electrode potential was proposed [12]. A similar method is also possible for our implementation, it is currently under construction.

For the moment being, we will use a simple approximate approach to estimate the electrode potential corresponding to a certain charge of the counter electrode and a given configuration of the considered system. We assume that the electrode potential at the electrochemical double layer reaches a stationary value already above the first water layer. We choose this location as the position z_{ref} at which all potential curves cross (see Fig. 6). The difference between the potential at this reference point and the Fermi energy can be regarded as a measure of the work function

$$\Phi = v(z_{ref}) - \varepsilon_F \quad (10)$$

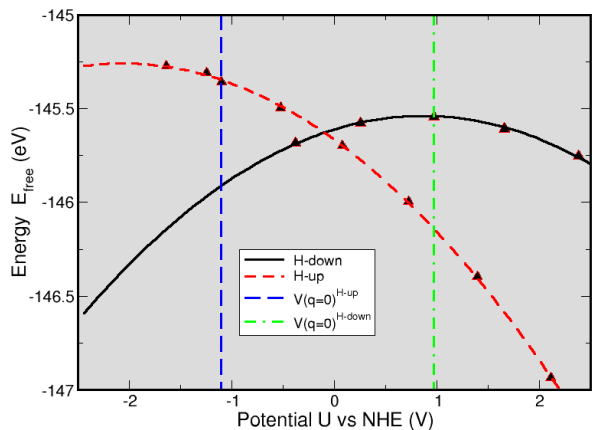


FIG. 7: Free energy (9) as a function of the electrode potential vs NHE for the H-up and H-down water layer on Pt(111). The curves correspond to a quadratic fit to the values (triangles) calculated for a $\sqrt{3} \times \sqrt{3}$ surface unit cell. In addition, the potential at zero excess charge corresponding to the work function is included.

The electrode potential U of the water-covered metal slab relative to the normal hydrogen electrode (NHE) can be estimated [12, 14, 62] by

$$U = \Phi - \Phi_{\text{NHE}}. \quad (11)$$

In the following, we will assume $\Phi_{\text{NHE}} = 4.44$ V [63]. We are aware that our procedure to specify the electrode potential is only approximate, however, here we will only present some preliminary results to demonstrate the usefulness of this implementation. In passing, we note that the fact that there are still several different approaches to model varying electrode potential is an indication that the first-principles description of electrochemical electrode-electrolyte interfaces is still in its infancy. This means that there is still room to develop new theoretical and numerical approaches which makes this field rather exciting.

As a first application, we will consider the stability of the H-up and H-down layer on Pt(111) as a function of the electrode potential. For water on Pd(111) [64] and on Pt/Au(111) [10], the transition between these two phases was already studied using DFT methods. Note, however, that these ice-like water structures are not stable at room temperature. In Fig. 7, the free energy (9) is plotted as a function of the electrode potential vs NHE for these two different water layers. Towards negative potentials, the range is limited in order to avoid the artificial electron transfer to the counter electrode for large positive charges.

The difference in the adsorption energies of the H-up and the H-down structure per water molecule without any applied electric field is only 0.04 eV [20]. Due to the strong difference in their work functions, these two structures are not at the same potential. The correspond-

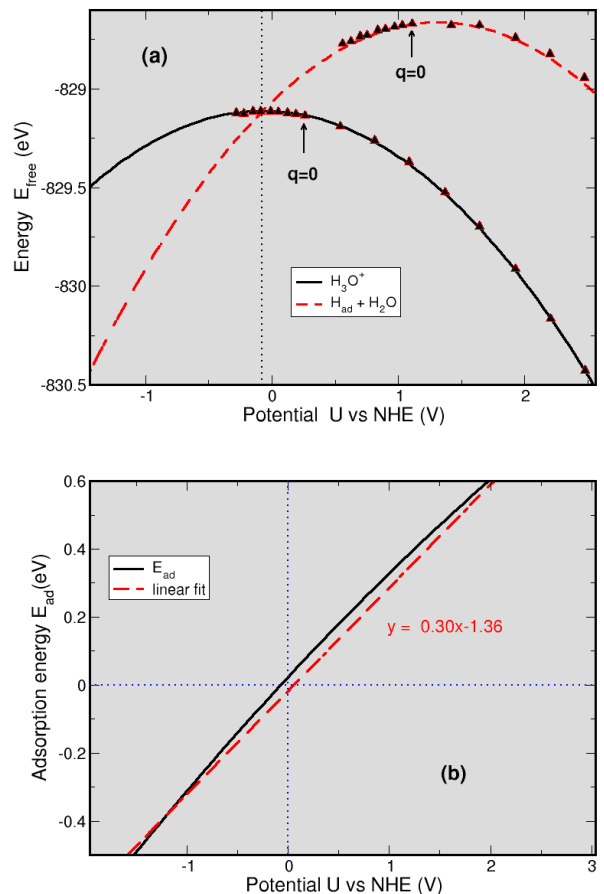


FIG. 8: (a) Free energy (9) as a function of the electrode potential vs NHE for a water bilayer on Pt(111) with an adsorbed hydrogen atom ($\text{H}_{\text{ad}} + \text{H}_2\text{O}$) and with a solvated proton in the water bilayer (H_3O^+). (b) Difference $E_{\text{free}}(\text{H}_{\text{ad}} + \text{H}_2\text{O}) - E_{\text{free}}(\text{H}_3\text{O}^+)$ between the two curves in (a) denoted as adsorption energy together with a linear fit.

ing values of the free energies are indicated by the perpendicular lines in Fig. 7. According to our calculations, above -0.06 V vs NHE, the H-up structure should be stable. This compares nicely with the value for Pd(111), where the phase transition occurs at -0.14 V vs NHE [64].

As a second example, we will address the Volmer reaction (2) $\text{H}_3\text{O}^+ + e^- \leftrightarrow \text{H}_{\text{ad}} + \text{H}_2\text{O}$, using an ice-like water bilayer on Pt(111) in a $2\sqrt{3} \times 2\sqrt{3}$ geometry. Without any external electric field, the adsorption of hydrogen on the metal electrode (H_{ad}) within this set-up is 0.23 eV less favorable than the incorporation of the hydrogen atom in the water bilayer leading to H_3O^+ .

The free energies of both structures as a function of the electrode potential vs NHE are plotted in Fig. 8(a). The difference $E_{\text{free}}(\text{H}_{\text{ad}} + \text{H}_2\text{O}) - E_{\text{free}}(\text{H}_3\text{O}^+)$ plotted in Fig. 8(b) can be regarded as an adsorption energy of the hydrogen atom with respect to a proton in solution. Apparently, the adsorption energy is approximately a linear function of the electrode potential. According to our

calculations, the equilibrium of the Volmer reaction is at about -0.08 V vs NHE, that means rather close to the equilibrium of the hydrogen evolution. This also means that the hydrogen evolution on Pt(111) with the intermediate adsorbed hydrogen state is essentially thermo-neutral. This has been recognized as an indication why Pt is an excellent catalyst for the hydrogen evolution [50].

V. CONCLUSIONS

There are quite significant challenges in the first-principles description of reactions in electrocatalysis due to the presence of the electrolyte at the electrode surface and varying electrode potentials. Still, the water/metal interface at finite temperatures can nowadays realistically be modeled using ab initio molecular dynamics simulations. Furthermore, there are different promising ap-

proaches to describe varying electrode potentials in periodic DFT calculations. We implemented a scheme in which a Gaussian-shaped planar counter electrode is explicitly considered and presented first results with respect to the hydrogen evolution on Pt(111). Although we still use a preliminary method to specify the corresponding electrode potential, our first results are in good agreement with previous theoretical studies.

Acknowledgments

This research has been supported by the Konrad-Adenauer-Stiftung. Computer time on the BW-Grid of the federal state of Baden-Württemberg is gratefully acknowledged. Useful discussions with Wolfgang Schmickler and Eckhard Spohr are gratefully acknowledged.

-
- [1] N. M. Marković and P. N. Ross Jr., *Surf. Sci. Rep.* **45** (2002) 117.
- [2] J. Rossmeisl, J. K. Nørskov, C. D. Taylor, M. J. Janik, and M. Neurock, *J. Phys. Chem. B* **110** (2006) 21833.
- [3] M. Koper, *Faraday Discuss.* **140** (2008) 11.
- [4] G. Kresse, M. Schmid, E. Napetschnig, M. Shishkin, L. Köhler, and P. Varga, *Science* **308** (2005) 1440.
- [5] R. T. Vang, K. Honkala, S. Dahl, E. K. Vestergaard, J. Schnadt, E. Lægsgaard, J. K. Clausen, B. S. Nørskov, and F. Besenbacher, *Nat. Mater.* **4** (2005) 160.
- [6] P. Jakob, K. Anhut, S. Schnur, and A. Groß, *Phys. Rev. Lett.* **101** (2008) 206101.
- [7] F. Eberle, M. Saitner, H.-G. Boyen, J. Kučera, A. Groß, A. Romanyuk, P. Oelhafen, M. D’Olieslaeger, M. Manolova, and D. M. Kolb, *Angew. Chem. Int. Ed.* **49** (2010) 341.
- [8] G. Mercurio, E. R. McNellis, I. Martin, S. Hagen, F. Leyssner, S. Soubatch, J. Meyer, M. Wolf, P. Tegeder, F. S. Tautz, and K. Reuter, *Phys. Rev. Lett.* **104** (2010) 036102.
- [9] A. Y. Lozovoi, A. Alavi, J. Kohanoff, and R. M. Lynden-Bell, *J. Chem. Phys.* **115** (2001) 1661.
- [10] A. Roudgar and A. Groß, *Chem. Phys. Lett.* **409** (2005) 157.
- [11] J. S. Filhol and M. Neurock, *Angew. Chem. Int. Ed.* **45** (2006) 402.
- [12] C. D. Taylor, S. A. Wasileski, J.-S. Filhol, and M. Neurock, *Phys. Rev. B* **73** (2006) 165402.
- [13] M. Otani and O. Sugino, *Phys. Rev. B* **73** (2006) 115407.
- [14] E. Skúlason, G. S. Karlberg, J. Rossmeisl, T. Bligaard, J. Greeley, H. Jónsson, and J. K. Nørskov, *Phys. Chem. Chem. Phys.* **9** (2007) 3241.
- [15] J. Zhao, C. T. Chan, and J. G. Che, *Phys. Rev. B* **75** (2007) 085435.
- [16] O. Sugino, I. Hamada, M. Otani, Y. Morikawa, T. Ikeshoji, and Y. Okamoto, *Surf. Sci.* **601** (2007) 5237.
- [17] M. Otani, I. Hamada, O. Sugino, Y. Morikawa, Y. Okamoto, and T. Ikeshoji, *Phys. Chem. Chem. Phys.* **10** (2008) 3609.
- [18] J. Rossmeisl, E. Skúlason, M. J. Björketun, V. Tripkovic, and J. K. Nørskov, *Chem. Phys. Lett.* **466** (2008) 68.
- [19] Y. Gohda, S. Schnur, and A. Groß, *Faraday Discuss.* **140** (2008) 233.
- [20] S. Schnur and A. Groß, *New J. Phys.* **11** (2009) 125003.
- [21] A. Michaelides, *Appl. Phys. A* **85** (2006) 415.
- [22] J. K. Nørskov, J. Rossmeisl, A. Logadottir, L. Lindqvist, J. R. Kitchin, T. Bligaard, and H. Jónsson, *J. Phys. Chem. B* **108** (2004) 17886.
- [23] G. Kresse and J. Furthmüller, *Phys. Rev. B* **54** (1996) 11169.
- [24] J. P. Perdew, K. Burke, and M. Ernzerhof, *Phys. Rev. Lett.* **77** (1996) 3865.
- [25] P. Vassilev, C. Hartnig, M. T. M. Koper, F. Frechard, and R. A. van Santen, *J. Chem. Phys.* **115** (2001) 9815.
- [26] J. VandeVondele, F. Mohamed, M. Krack, J. Hutter, M. Sprik, and M. Parrinello, *J. Chem. Phys.* **122** (2005) 014515.
- [27] B. Santra, A. Michaelides, M. Fuchs, A. Tkatchenko, C. Filippi, and M. Scheffler, *J. Chem. Phys.* **129** (2008) 194111.
- [28] P. E. Blöchl, *Phys. Rev. B* **50** (1994) 17953.
- [29] G. Kresse and D. Joubert, *Phys. Rev. B* **59** (1999) 1758.
- [30] A. Groß, *Surf. Sci.* **363** (1996) 1.
- [31] M. Lischka and A. Groß, *Phys. Rev. B* **65** (2002) 075420.
- [32] G.-J. Kroes, A. Groß, E. J. Baerends, M. Scheffler, and D. A. McCormack, *Acc. Chem. Res.* **35** (2002) 193.
- [33] A. Roudgar and A. Groß, *J. Electroanal. Chem.* **548** (2003) 121.
- [34] A. Roudgar and A. Groß, *Surf. Sci.* **559** (2004) L180.
- [35] A. Groß, *Topics Catal.* **37** (2006) 29.
- [36] L. A. Kibler, *Chem. Phys. Chem.* **7** (2006) 985.
- [37] J. M. Heras and L. Viscido, *Appl. Surf. Sci.* **4** (1980) 238.
- [38] E. Langenbach, A. Spitzer, and H. Lüth, *Surf. Sci.* **147** (1984) 179.
- [39] M. Kiskinova, G. Pirug, and H. Bonzel, *Surf. Sci.* **150** (1985) 319.
- [40] W. Hoffmann and C. Benndorf, *Surf. Sc.* **377-379** (1997) 681.
- [41] Y. Lilach, L. Romm, T. Livneh, and M. Asscher, *J. Phys. Chem. B* **105** (2001) 2736.

- [42] P. J. Feibelman, *Science* **295** (2002) 99.
- [43] G. Materzanini, G. F. Tantardini, P. J. D. Lindan, and P. Saalfrank, *Phys. Rev. B* **71** (2005) 155414.
- [44] D. Menzel, *Science* **295** (2002) 58.
- [45] C. Clay, S. Haq, and A. Hodgson, *Chem. Phys. Lett.* **388** (2004) 89 .
- [46] A. Groß and A. Dianat, *Phys. Rev. Lett.* **98** (2007) 206107.
- [47] P. Vassilev, C. Hartnig, M. T. M. Koper, F. Frechard, and R. A. van Santen, *J. Chem. Phys.* **115** (2001) 9815.
- [48] C. Hartnig and M. T. M. Koper, *J. Chem. Phys.* **115** (2001) 8540.
- [49] A. Roudgar and A. Groß, *Surf. Sci.* **597** (2005) 42.
- [50] J. K. Nørskov, T. Bligaard, A. Logadottir, J. R. Kitchin, J. G. Chen, S. Pandelov, and U. Stimming, *J. Electrochem. Soc.* **152** (2005) J23.
- [51] T. Bligaard, K. Honkala, A. Logadottir, J. K. Nørskov, S. Dahl, and C. J. H. Jacobsen, *J. Phys. Chem. B* **107** (2003) 9325.
- [52] N. M. Marković, T. J. Schmidt, B. N. Grgur, H. A. Gasteiger, R. J. Behm, and P. N. Ross, *J. Phys. Chem. B* **103** (1999) 8568.
- [53] K. Christmann, *Surf. Sci. Rep.* **9** (1988) 1.
- [54] K. Kunimatsu, T. Senzaki, M. Tsushima, and M. Osawa, *Chem. Phys. Lett.* **401** (2005) 451.
- [55] J. Neugebauer and M. Scheffler, *Phys. Rev. B* **46** (1992) 16067.
- [56] S. A. Wasileski and M. J. Janik, *Phys. Chem. Chem. Phys.* **10** (2008) 3613.
- [57] M. Neurock, M. Janik, and A. Wiechowski, *Faraday Discuss.* **140** (2008) 363.
- [58] C. L. Fu and K. M. Ho, *Phys. Rev. Lett.* **63** (1989) 1617.
- [59] K. P. Bohnen and D. M. Kolb, *Surf. Sci.* **407** (1998) L629.
- [60] A. Y. Lozovoi and A. Alavi, *Phys. Rev. B* **68** (2003) 245416.
- [61] J. G. Che and C. T. Chan, *Phys. Rev. B* **67** (2003) 125411.
- [62] S. Trasatti, *Surf. Sci.* **335** (1995) 1.
- [63] S. Trasatti, *Pure Appl. Chem.* **58** (1986) 955.
- [64] J. S. Filhol and M.-L. Bocquet, *Chem. Phys. Lett.* **438** (2007) 203.